Ultimate Capacity of a Laser Diode in Transporting Multichannel M-QAM Signals

Pi-Yang Chiang, *Student Member, IEEE*, and Winston I. Way, *Senior Member, IEEE*

***Abstract*— In this paper, we investigate the ultimate M-ary quadrature amplitude modulated (M-QAM) channel capacity of a laser diode which is limited by the laser clipping induced nonlinear distortions. Our study includes a spectral analysis, a complete system simulation, and an experiment which used up to 70 channels of vector arbitrary waveform synthesizer generated quadrature phase shift keyed (QPSK) or 16-QAM signals to modulate an isolated/cooled distributed-feedback (DFB) laser and two unisolated/uncooled Fabry–Perot (FP) lasers, respectively. Our analytical results show that for an upstream laser diode, over 1000 QPSK channels or 170 16-QAM channels can be delivered, even in the presence of a high relative intensity noise (RIN) of -115 dB/Hz. However, these high capacities are reduced significantly when we consider the effect of collision-based medium access control (MAC) protocols. We found that, in the worst case condition (collisions occur in all but one channels), the ultimate QPSK channel capacity of an upstream laser diode is dramatically reduced from over 1000 to 125 for eight collisions/channel. These results have important implications to systems transporting frequency-stacked return-path bands with or without collision-based MAC channels. As regard to the ultimate capacity of a down-stream laser diode with a RIN level of -135 dB/Hz, we found that as high as 600 and 128 channels of 64-QAM and 256-QAM signals (equivalent to 3600 and 1152 channels of MPEG-II live video signals) can be transported, respectively.**

***Index Terms*— Cable TV, clipping, hybrid fiber/coax, laser diode, M-QAM, nonlinear distortion.**

I. Introduction

FUTURE hybrid-fiber coax (HFC) systems for bidirectional communications would require high channel capacities in both upstream and downstream optical fiber links. However, the capacity of a directly modulated laser diode is always limited by laser clipping. Consequently, the channel capacity and clipping-induced nonlinear distortions (NLD's) in a *downstream* laser which transports multichannel AM–VSB video signals have been extensively studied [1]-[6]. The dominant traffic load on an *upstream* laser, on the other hand, would be M-QAM modulation-based Internet access, video on demand, cable telephony, etc., [7]. These intense multimedia traffic in combination with frequency stacking technique [8] can impose a high capacity requirement on a single upstream laser [9], [10]. The frequency stacking technique is illustrated in Fig. 1. By frequency multiplexing N return-path spectra

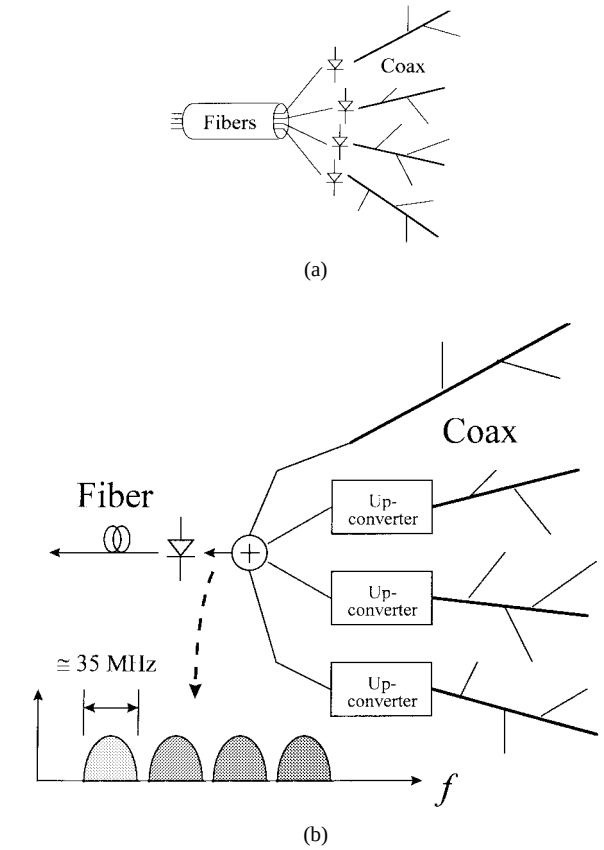

Fig. 1. (a) Using N upstream lasers and N fibers to carry N return-path band signals. (b) Using a single laser and a single fiber to carry N frequency-stacked return-path bands.

(each between 5 to ~40 MHz), we can save $N-1$ laser diodes and $N-1$ optical fibers. Furthermore, the channel capacity of an upstream laser may be decreased due to the collision-based medium access control (MAC) protocols which Internet access and video on demand will use [7]. With the motivations mentioned above, the main goal of this paper is to study the ultimate channel capacity of an upstream laser diode, although the same analytical and simulation techniques are also applied to downstream laser diodes which carry multichannel M-QAM signals.

We shall approach the problem by using a spectral analysis, computer simulations, and experimental verifications. The spectral analysis, presented in Section II, is based on modeling the composite input signal as a Gaussian random process, and using the series expansion of the output autocorrelation function [3], [6], [11] resulted from laser clipping to obtain

Manuscript received March 24, 1997; revised June 23, 1997. This work was supported by the National Science Council, R.O.C., under Contract NSC85-2622-E009-015.

The authors are with the Department of Communication Engineering National Chiao-Tung University Hsinchu, Taiwan, R.O.C.

Publisher Item Identifier S 0733-8724(97)07539-7.

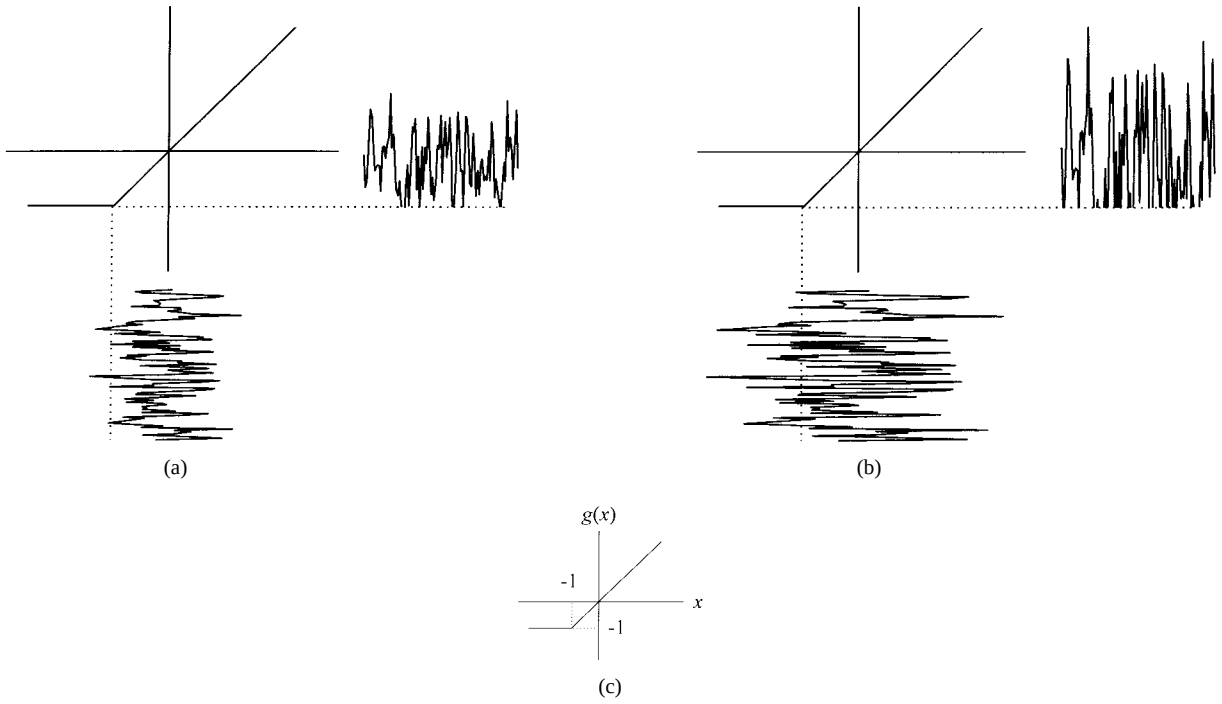

Fig. 2. (a) Laser diode under weak clipping, (b) laser diode under strong clipping, and (c) normalized nonlinear transfer function of a linear laser diode.

output power spectral density (PSD) [2], [5], [12]. Note that we shall concentrate on the case of *strong* laser clipping as opposed to *weak* laser clipping because the SNR requirement on M-QAM signals is much lower than that on AM–VSB signals. Fig. 2(a) and (b) illustrates the basic concept of strong clipping and weak clipping, respectively. The computer simulations, which are based on an ideal L-I transfer function and an ideal M-QAM modem with pulse shaping filters (with a perfect carrier recovery and a synchronized timing recovery), are presented in Section III. In our experiments, presented in Section IV, up to 70 channels of M-QAM signals were used to modulate various types of laser diodes (cooled/uncooled, isolated/unisolated Fabry–Perot (FP) and DFB), and the results were used to verify the analytical and simulation results. Ultimate upstream channel capacity estimation was given based on 1 Ms/s per channel. Section V covers the effects of collision-based MAC protocols on the reduction of channel capacity, and the ultimate M-QAM channel capacity of a downstream laser diode (based on 5 Ms/s/channel). Section VI concludes the paper.

II. Analysis

If the number of channels in a subcarrier multiplexed lightwave transmission system is large and all the channels have nearly equal root-mean-square (rms) power, the multiplexed signal can be approximated as a Gaussian random process. In the case of upstream links, equal power channels can be achieved by sending control information from headend to the automatic gain control circuit in each subscriber's modem, although Section V shows that the analysis can also be applied to estimate the dynamic range of unequal input signal powers under the worst condition. The second-order density of a zero-mean Gaussian process can be expanded as a power series of normalized autocorrelation function $\rho(\tau)$ as [11], [12]

$$f(x_1,x_2)=\frac{1}{2\pi\sigma^2}\,\exp\left[-\frac{x_1^2+x_2^2}{2\sigma^2}\right]\cdot\sum_{n=0}^{\infty}\frac{\rho^n(\tau)}{n!}\,H_n\Big(\frac{x_1}{\sigma}\Big)\,H_n\Big(\frac{x_2}{\sigma}\Big) \tag{1}$$

where $x_1=x(t_1),\quad x_2=x(t_2),\quad \tau=t_2-t_1$, and σ^2 is the variance of the Gaussian process. $R_x(\tau)=\sigma^2\cdot\rho(\tau)$ is the autocorrelation function of the input signal, $H_n(x)$ is the nth order Hermite function which is defined as

$$H_n(x)=(-1)^n e^{\frac{x^2}{2}}\frac{d^n}{dx^n}e^{-\frac{x^2}{2}}. \tag{2}$$

Assume the transfer function of the lightwave transmission system is $y=g(x)$, the output autocorrelation function is given by

$$R_y(t_1,t_2)=E[y(t_1)y(t_2)]=\int_{-\infty}^{\infty}\int_{-\infty}^{\infty}f(x_1,x_2)\,g(x_1)\,g(x_2)\,dx_1\,dx_2. \tag{3}$$

By substituting (1) into (3), we obtain

$$\begin{aligned}R_y(t_1,t_2)&=\int_{-\infty}^{\infty}\int_{-\infty}^{\infty}\frac{1}{2\pi\sigma^2}\,\exp\left[-\frac{x_1^2+x_2^2}{2\sigma^2}\right]\cdot\sum_{n=0}^{\infty}\frac{\rho^n(\tau)}{n!}\,H_n\Big(\frac{x_1}{\sigma}\Big)\,H_n\Big(\frac{x_2}{\sigma}\Big)\,g(x_1)\cdot g(x_2)\,dx_1\,dx_2\\&=\sum_{n=0}^{\infty}\frac{\rho^n(\tau)}{n!}\left[\frac{1}{\sqrt{2\pi}}\int_{-\infty}^{\infty}g(\sigma x)\,e^{-\frac{x^2}{2}}\,H_n(x)\,dx\right]^2\\&=\sum_{n=0}^{\infty}\frac{\rho^n(\tau)}{n!}\,b_n^2\end{aligned} \tag{4}$$

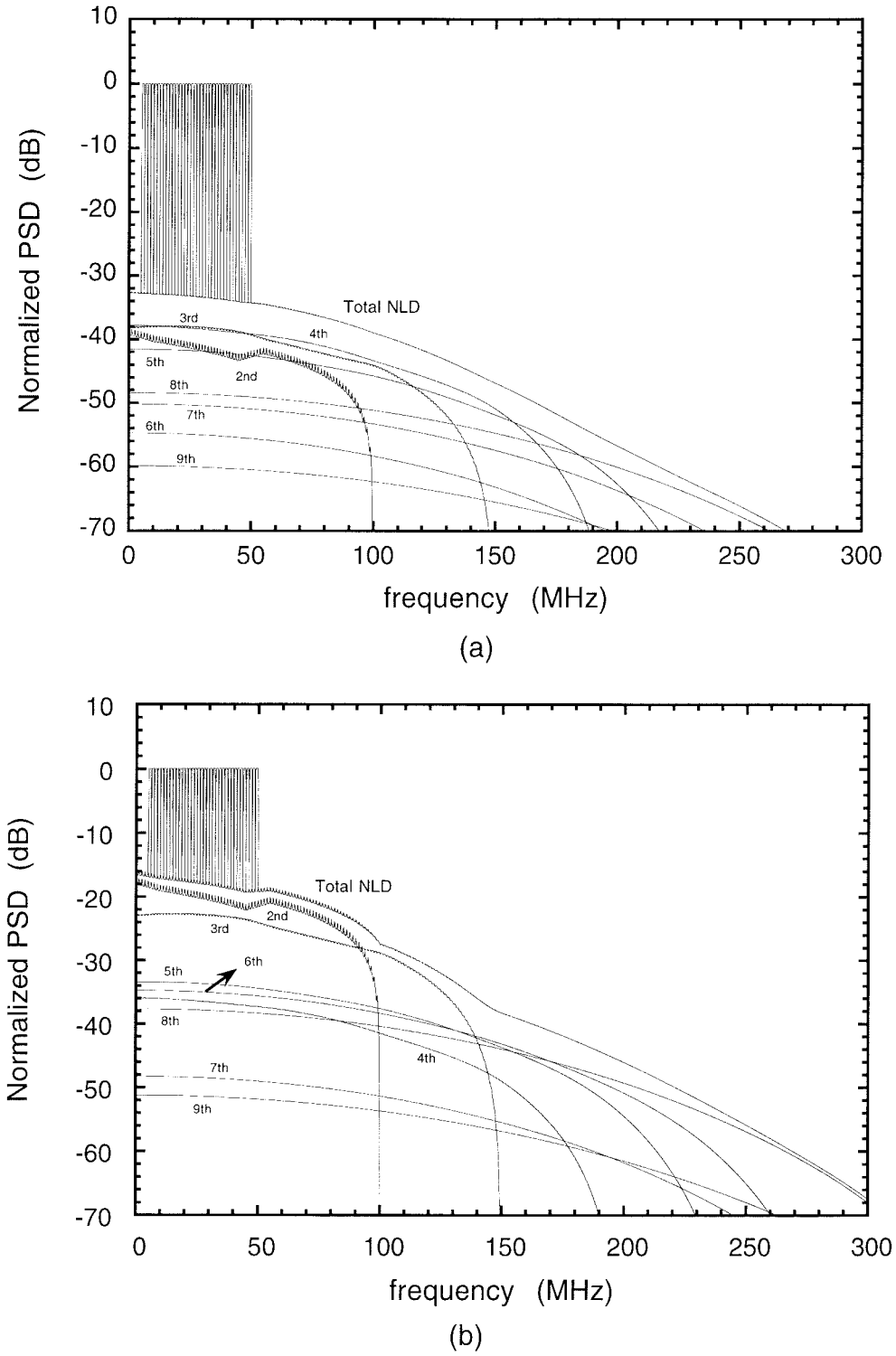

Fig. 3. Calculated spectral distribution of clipping-induced second, third, $\cdots$, nineth-order NLD's. Thirty-six channels of M-QAM channels with RRC filtering are used. (a) $\mu = 0.4$ and (b) $\mu = 0.8$.

where b_n is defined as

$$b_n \equiv \frac{1}{\sqrt{2\pi}} \int_{-\infty}^{\infty} g(\sigma x)\, e^{-\frac{x^2}{2}}\, H_n(x)\, dx\,, \qquad n \geq 0. \quad (5)$$

For a laser diode with normalized L-I transfer function $g(x)$ shown in Fig. 2(c), $\sigma = \mu = \sqrt{N} \cdot m$, and b_n can be evaluated as

$$b_n = \begin{cases} -\frac{1}{2}\,\mathrm{erfc}\left(\frac{1}{\sqrt{2}\sigma}\right) + \frac{\sigma}{\sqrt{2\pi}} e^{-\frac{1}{2\sigma^2}} & n = 0 \\ \frac{\sigma}{2}\,\mathrm{erfc}\left(-\frac{1}{\sqrt{2}\sigma}\right) & n = 1 \\ \frac{\sigma}{\sqrt{2\pi}} H_{n-2}\left(-\frac{1}{\sigma}\right) e^{-\frac{1}{2\sigma^2}} & n \geq 2 \end{cases} \quad (6)$$

where μ is the total rms optical modulation index (OMI), N is the number of channels, and m is the rms OMI per channel.

Note that the rms OMI is used here instead of peak OMI because the peak amplitude of an M-QAM signal varies not only with M, but also with the characteristics of the pulse shaping filter.

The output power spectral density (PSD) $S_y(f)$ is the Fourier transform of the autocorrelation function $R_y(\tau)$

$$\begin{aligned} S_y(f) &= \int_{-\infty}^{\infty} R_y(\tau)\, e^{-j2\pi f\tau}\, d\tau \\ &= \sum_{n=0}^{\infty} \frac{b_n^2}{n!} \int_{-\infty}^{\infty} \rho^n(\tau)\, e^{-j2\pi f\tau}\, d\tau \\ &= \sum_{n=0}^{\infty} \frac{b_n^2}{n!}\, \varphi^{(n)}(f) \end{aligned} \tag{7}$$

where $\varphi^{(1)}(f) = \int_{-\infty}^{\infty} \rho(t)\, e^{-j2\pi ft} dt$ is the normalized input PSD, and

$$\varphi^{(n)}(f) = \underbrace{\varphi^{(1)}(f) \otimes \varphi^{(1)}(f) \otimes \cdots\cdots \otimes \varphi^{(1)}(f)}_{n}$$

is the $n-1$ times self-convolution of $\varphi^{(1)}(f) (n \geq 2)$. Note that the first term $b_0^2\varphi^{(0)}(f)$ in the summation of (7) represents dc component in the spectrum. The second term $(n = 1) b_1^2\varphi^{(1)}(f)$ is the signal component in the output spectrum with attenuation $20\cdot\log(b_1)$ dB compared to the input signal. The rest of terms ($n \geq 2$) represent the second to higher order nonlinear distortion powers due to the ideal L-I curve. Suppose we use root raised-cosine (RRC) filter as the pulse shaping filter, the PSD of a baseband QAM signal after filtering can be expressed as (8) shown at the bottom of the page where T is the symbol period and α is the roll-off factor of the filter. In an N-channel M-QAM system, the overall input PSD is given by

$$S_x(f) = \sum_{i=1}^{N} [S(f - f_i) + S(f + f_i)] \tag{9}$$

where f_i is the center frequency of the ith channel and N denotes the number of channels, and the normalized input PSD is

$$\varphi^{(1)}(f) = \frac{S_x(f)}{\int_{-\infty}^{\infty} S_x(f) df}. \tag{10}$$

By using (6)–(10) and let the input spectrum consist of 36 channels from 5 to 50 MHz with a channel spacing = 1.25 MHz, a symbol rate = 1 Ms/s, and $\alpha = 0.2$, we can obtain the calculated clipped spectra for rms OMI $\mu = 0.4$ and 0.8 as shown in Fig. 3(a) and (b), respectively. Several interesting phenomena can be observed. 1) There are wiggles in the second and third order nonlinear distortion spectra, owing to the fact that there are filtered notches among input QAM channels. As for higher orders, the wiggles disappear due to more convolutional averages. 2) The highest frequency of the nth order nonlinearity is n-fold of the maximum frequency (50 MHz) of the input spectrum. 3) The left-most channel (channel#1) always has the highest total NLD power. 4) Lower order NLD power is not always higher than that of higher orders. For example, when $\mu = 0.4$, the fourth NLD power is greater than that of the second order. The same fact can be observed for $\mu = 0.8$ where the sixth NLD power is greater than that of the fourth order. This phenomenon can be explained as follows.

The signal-to-nonlinear distortions ratio (SNLD) of the ith channel centered at frequency f_i and with a bandwidth $2\Delta f$ can be obtained from dividing the integrated signal PSD ($b_1^2\varphi(1)(f)$) by the total integrated NLD PSD [from (7)]

$$\mathbf{SNLD}_i = \frac{b_1^2 \int_{f_i-\Delta f}^{f_i+\Delta f} |H(f)|^2\, \varphi^{(1)}(f)\, df}{\sum_{n=2}^{\infty} \frac{b_n^2}{n!} \int_{f_i-\Delta f}^{f_i+\Delta f} |H(f)|^2 \varphi^{(n)}(f)\, df} \tag{11}$$

where $H(f)$ is the transfer function of the receiver filter. The signal to a specific nth order NLD ratio for the ith channel, $\mathbf{SNLD}_i^N$, can be easily resolved from (11). The calculated $\mathbf{SNLD}_i^N$ ($n = 2, 3, \cdots, 9$) with a RRC receiver filter ($\alpha = 0.2$), are plotted in Fig. 4. Fig. 4 shows that SNLD in channel#1 (the worst case channel) varies with μ for different orders of NLD's and $N = 36$. Note that there are spikes in each $\mathbf{SNLD}_i^N$ which represent singularities caused by $b_n = 0$ ($n = 2, 3, \cdots, 9$) for certain values of μ . It can be observed from Fig. 4 that the second and third NLD's are not dominant terms for $\mu \leq 0.45$. In fact, as μ decreases toward zero, the order of the dominant NLD increases.

Based on (11), we can also show that as long as the electrical driving power to a laser diode is kept constant, i.e., by keeping μ constant, the resultant SNLD changes little with the number of loading channels N (for N greater than about ten) as shown in Fig. 5. This phenomenon was previously pointed out in [13].

We would like to compare our analytical results with the modified Saleh's formula [14] given as follows:

$$\mathbf{CNLD} = \frac{1}{\Gamma} \sqrt{\frac{\pi}{2}}\, \frac{1 + 6\mu^2}{\mu^3}\, e^{\frac{1}{2\mu^2}}. \tag{12}$$

First of all, we note that the in-band correction factor Γ in (12) is dependent on μ and the number of loading channels N instead of being a constant. Discussions on this dependence using the asymptotic approach was given previously [4], but that approach is only applicable to small μ (< 0.25). Here we provide an accurate calculation of μ- and N-dependent Γ by using

$$\Gamma = \frac{\sum_{n=2}^{\infty} \frac{b_n^2}{n!} \int_{f_a}^{f_b} \varphi^{(n)}(f)\, df}{\sum_{n=2}^{\infty} \frac{b_n^2}{n!} \int_{0}^{\infty} \varphi^{(n)}(f)\, df} \tag{13}$$

$$S(f) = \begin{cases} 1, & |fT| < \frac{1}{2}(1-\alpha) \\ \frac{1}{2}\left[1 + \cos\left(\frac{\pi}{\alpha}(|fT| - \frac{1}{2}(1-\alpha))\right)\right], & \frac{1}{2}(1-\alpha) < |fT| < \frac{1}{2}(1+\alpha) \\ 0, & |fT| > \frac{1}{2}(1+\alpha) \end{cases} \tag{8}$$

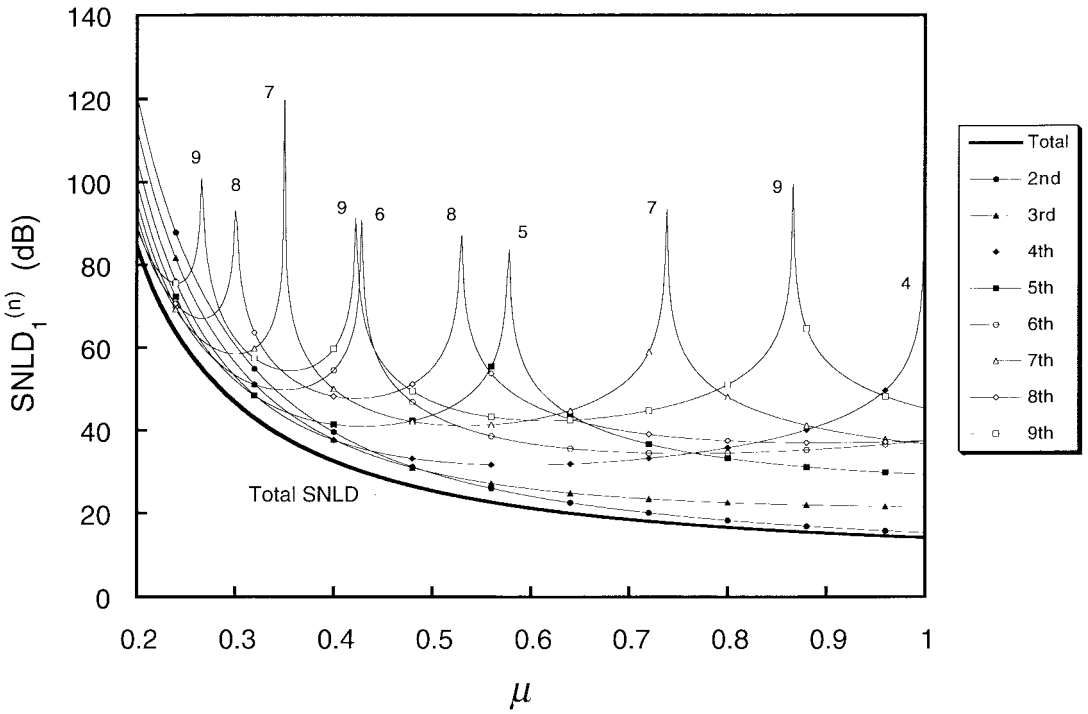

Fig. 4. SNLD of channel#1 (due to various order of NLD's) as a function of μ for $N = 36$.

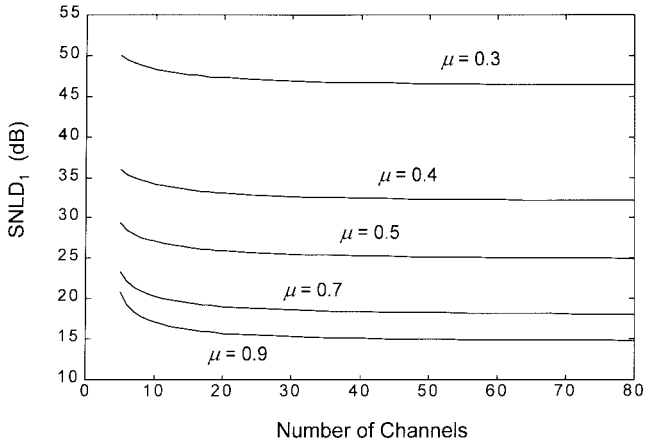

Fig. 5. SNLD as a function of N with various values of μ.

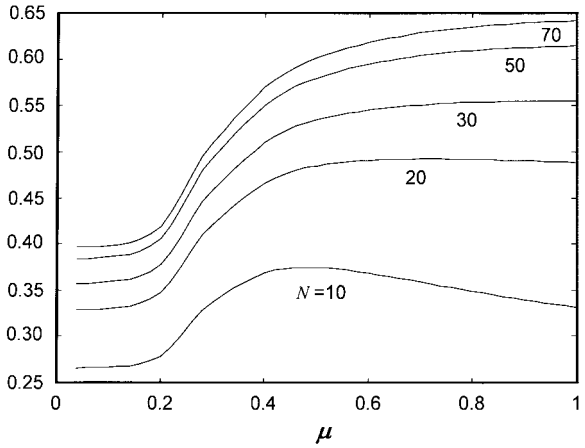

Fig. 6. Γ as a function of μ with various values of N.

where b_n is a function of μ, $\varphi^{(n)}(f)$ is a function of N, f_a and f_b are the minimum and maximum frequencies of the input signal, respectively. Fig. 6 shows Γ as a function of N and μ. It can be seen that the value of Γ can be as low as 0.27, or as high as 0.64, depending on the values of N and μ. We note that as the number of channels increases, higher fraction of NLD will fall into the composite signal band; and Γ increases faster for lower μ than for higher μ.

Now we can plug this accurately calculated Γ into (12) and obtain the results (shown by the solid line in Fig. 7) of SNLD for all channels as a function of μ ($N = 36$). Since (12) assumes that the input spectrum is flat between f_a and f_b, we can also use our analytical approach [see (11)] by assuming a flat input signal spectrum to obtain an SNLD(μ) without receiver filtering, mainly for the purpose of comparison. SNLD(μ)'s were calculated for the worst case channel, i.e., channel#1 (shown by solid circles in Fig. 7) and for channel#36 (shown by open circles in Fig. 7). We can see that the SNLD's obtained from (12) with calibrated Γ fall right between those of channel#1 and channel#36 by using our analysis. This is a very reasonable match because (12) considers the average SNLD among all channels (17).

Next, we assume a more realistic input spectrum which is composed of 36 channels of root-raised cosine filtered M-QAM signals. By using (11) we can obtain results for channel#1 (shown by the open squares in Fig. 7) and for channel#36 (shown by solid squares in Fig. 7). It can be observed that the calibrated Saleh's results happen to match well with the SNLD of channel#1, but differ from those of channel#36 by as much as 2.7 dB.

Another interesting phenomenon which can be observed from Fig. 7 is that even when μ is as high as 0.8, it is still

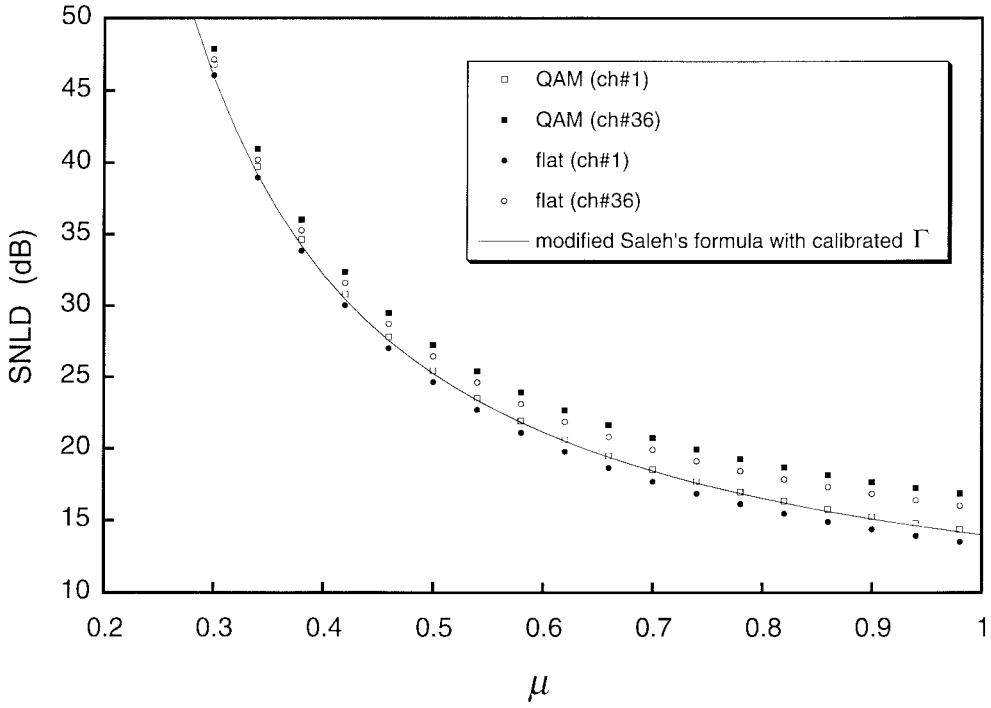

Fig. 7. SNLD as a function of μ for $N = 36$. Squares and circles are obtained from 36 RRC filtered QAM input signals and an input signal with a flat spectrum, respectively. The solid line is calculated from the modified Saleh's formula with calibrated Γ.

possible to maintain an SNLD $>$ 16 dB. Therefore, we should be able to obtain error-free transmission for upstream QPSK signals provided the NLD's can be treated as Gaussian noise (so that we have SNR $>$ 16 dB). This fact was confirmed in our experiment, which will be described in Section V.

III. Simulation

The simulation system block diagram is shown in Fig. 8. For each of the QPSK or 16-QAM channels, 1000 1-Ms/s random baseband pulse-amplitude-modulation (PAM) symbols with M levels were generated where M equals 4 and 16 for QPSK and 16-QAM, respectively. After the constellation mapping, the symbols were split into I and Q channels. The I and Q data were then band-limited by RRC filters ($\alpha = 0.2$). Note that an inverse sinc equalizer was cascaded before each RRC filter to equalize the spectrum of the NRZ pulses. The filtered baseband waveform were then quadrature modulated (with a random carrier phase) to the center frequency of a particular channel. In addition, a delay (varying between 0 to T for different channels) was added to simulate random clock phase of each channel, where T is the symbol period. Ten to 70 such channels were generated and then summed together. The band-edge of the first channel was at 5 MHz, and the channel spacing was 1.25 MHz. The sampling frequency for the baseband signal was 125 MHz, but was increased to at least ten fold of the right edge of the multiplexed signal (in order to accommodate up to the fifth-order distortions) after up-converting each QAM signal to its center frequency.

The combined up-converted signals were then clipped by a normalized ideal L-I curve as shown in Fig. 2(c). At the receiver, each QAM signal was first demodulated by quadrature down-converting the channel to baseband, and then passed through I/Q RRC filters ($\alpha = 0.2$). We assume ideal carrier and clock recovery so that each symbol can be sampled at the optimum point. The received average signal-to-noise ratio (SNR) can be computed by comparing the sampled constellation to the ideal constellation. This can be done by observing that the average power of the QAM signal is given by (see Fig. 9 for illustration)

$$P_{av} = \frac{2}{3}(M-1)\,d^2 \tag{14}$$

where d is half of the minimum constellation distance. Therefore, the channel SNR is given by

$$\text{SNR} = \frac{P_{av}}{< e^2 >} \tag{15}$$

where e is the error magnitude. The simulation results will be presented together with the experimental results in the next section.

IV. Experiment

We shall describe our experiment in terms of two parts: 1) a novel technique for generating multichannel M-QAM signals, and 2) a system experiment by using various types of laser diodes.

A. Generation of Multichannel M-QAM Signals

As shown in Fig. 10, we converted the digital data from computer simulation into real RF signals by a vector arbitrary waveform synthesizer (VAWS), which consists of a vector modulator and two 125 MHz, 12-bit digital-to-analog converters (DAC's) [10], [15], [16]. The bandwidth of the low-pass filter after each DAC is 50 MHz. The underlying

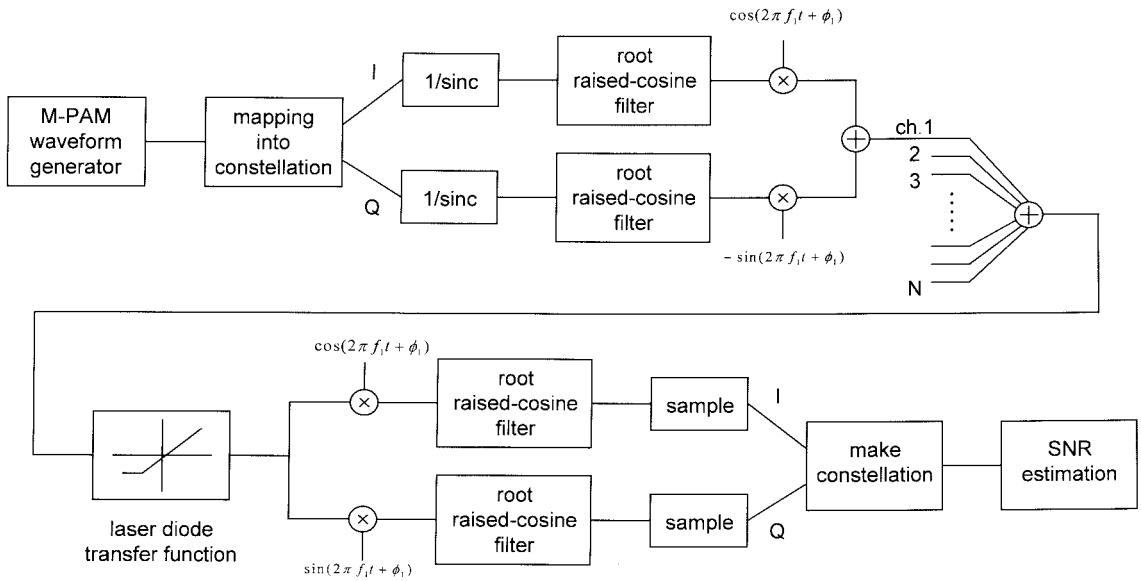

Fig. 8. Computer simulation block diagram

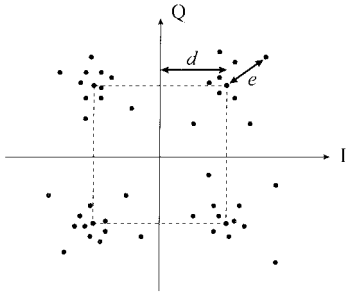

Fig. 9. Illustration of the magnitude of the error vector and the decision distance in a constellation diagram.

principle of Fig. 10 can best be illustrated by an example which shows how 70 channels of M-QAM signals are generated: in the computer program, each complex baseband QAM signal $s_i(t) = I_i(t) + j\ Q_i(t)$ $(i = 1, 2, \cdots, 70)$ is frequency shifted to a temporary center frequency f_i' by multiplying with $\exp(2\pi\ f_i'\ t + \phi_i))$. Seventy such complex frequency shifted signals are then combined to form a composite signal $v(t)$ whose frequency spectrum is shown in Fig. 10. Note that if we had used "real" frequency shifting (by multiplying each $s_i(t)$ with $\cos(2\pi\ f_i'\ t + \phi_i)$ instead of "complex" frequency shifting, we could obtain only 35 instead of 70 distinct channels. Note also that it is important to minimize the number of cloned channels to avoid artificially increased clipping probabilities. The complex composite signal $v(t)$ can be written as shown in (16) at the bottom of the next page where $I(t)$ and $Q(t)$ are the real and imaginary part of the download data $v(t)$, respectively. The real and imaginary parts of $v(t)$ were then downloaded to the memories of VAWS for digital to analog conversion and quadrature up-conversion, and the output $u(t)$ is given by (17) shown at the bottom of the next page where f_c and f_i are the center of the signal band and the center frequency of the ith channel, respectively Therefore, 70 distinct, real M-QAM channels are finally obtained. The first channel starts at 5 MHz, and the last channel ends at 5+1.25 $\times$ 70 $=$ 92.5 MHz.

To simulate bursty M-QAM channel, the burst time slots set by the computer program are such that the burst length and the guard time of each channel were 246 and four symbols, respectively, as illustrated in Fig. 10. The rise and fall time of the burst were both about 8 ns which is much shorter than that set by the standard bodies [7].

B. Upstream System Experiment

Two uncooled, unisolated FP lasers and a cooled, isolated DFB laser were tested. The output power of the three lasers were set at 0.4, 0.5, and 1 mW, respectively. For a given number of channels in the modulating signal, the OMI of each channel was increased to its upper limit until the power level of nonlinear distortions reached a given threshold. Note that the NLD can be treated as Gaussian noise because the laser was driven under a "strong" clipping condition. This is different from the multichannel AM–VSB case where the "weak" clipping-induced noise is impulsive rather than Gaussian. We verify this fact by adding a commercially available QAM modem to the edge of the previously generated 70 channels, and note that effect of multichannel QAM-induced NLD's on the bit error rate (BER) performance is the same as that of externally added Gaussian noise (by using a noise and interference test set, HP3708A).

A typical result is shown in Fig. 11(a) where 70 channels of 16-QAM signals were used to drive FP laser#2 into deep clipping. We can see that the SNR requirement of 24 dB can be maintained for all channels (with clear constellation and eye diagrams) when OMI/ch $\leq$ 6.86%, while the constellation and eye diagrams collapsed when OMI/ch exceeded 6.86%. Also note that when the laser is strongly-clipped (OMI/ch $=$ 6.86%), the transient-induced spectral regrowth, which is caused by the fast turn-on and -off of the bursty signals, became insignificant as compared to the NLD's. This phenomenon can be seen at the left edge of channel#1 [Fig. 11(b)].

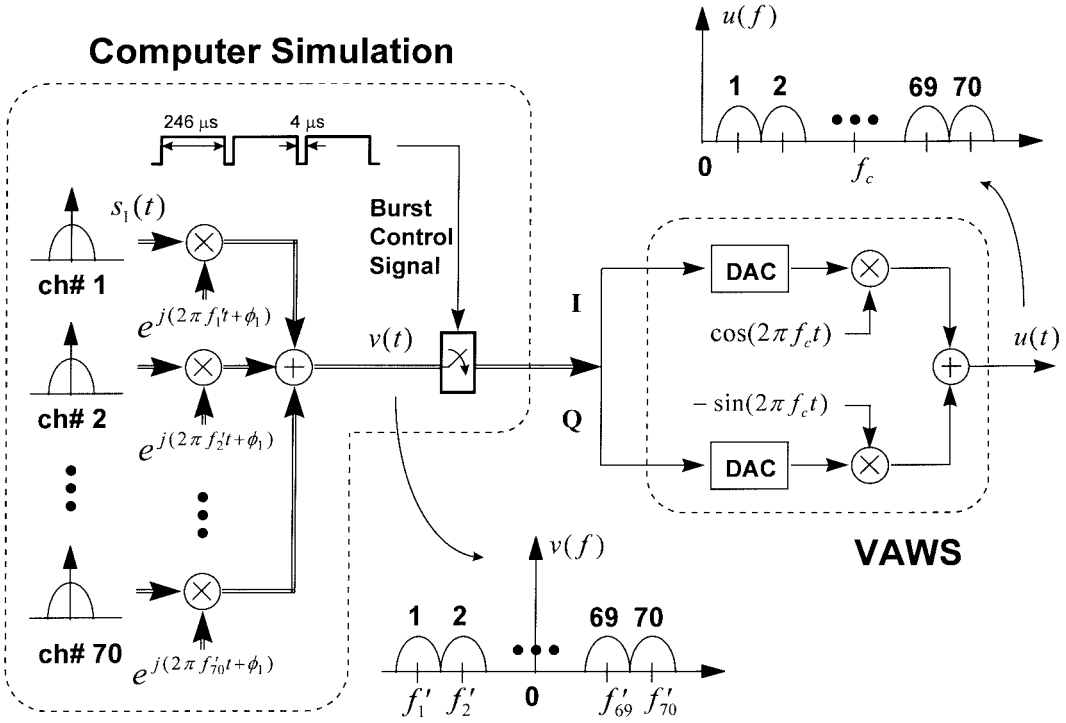

Fig. 10. Experimental technique in generating 70 channels of M-QAM signals by using a computer software and a vector arbitrary waveform synthesizer (VAWS).

Fig. 12 shows the measured, computer simulated, and calculated ultimate channel number as a function of OMI per channel. The total channel number was increased from 10 to 70 in a step-size of 10 during the experiment, and the worst-case channel, channel#1, must reach the minimum required SNR of 16 or 24 dB. At these SNR thresholds, the BER of the QAM signal can be well below 10^{-9}. The useful OMI/ch values are bounded by two sides: the maximum OMI/ch is limited by the strong-clipping-induced NLD's, and the minimum OMI/ch is limited by the large relative intensity noise (RIN)

$$\begin{aligned} v(t) &= \sum_{i=1}^{70} s_i(t)\cdot e^{j(2\pi f_i' t+\phi_i)} \\ &= \sum_{i=1}^{70} [I_i(t)+j\ Q_i(t)]\cdot[\cos(2\pi f_i' t+\phi_i)+j\ \sin(2\pi f_i' t+\phi_i)] \\ &= \sum_{i=1}^{70} [I_i(t)\cos(2\pi f_i' t+\phi_i) - Q_i(t)\sin(2\pi f_i' t+\phi_i)] \\ &\quad + j\sum_{i=1}^{70} [I_i(t)\sin(2\pi f_i' t+\phi_i) + Q_i(t)\cos(2\pi f_i' t+\phi_i)] \\ &\equiv I(t)+j\ Q(t) \end{aligned} \tag{16}$$

$$\begin{aligned} u(t) &= I(t)\cos(2\pi f_c t) - Q(t)\sin(2\pi f_c t) \\ &= \sum_{i=1}^{70} [I_i(t)\cos(2\pi(f_c+f_i')t+\phi_i) - Q_i(t)\sin(2\pi(f_c+f_i')t+\phi_i)] \\ &= \sum_{i=1}^{70} \mathrm{Re}\left\{[I_i(t)+j\ Q_i(t)]\ e^{j(2\pi(f_c+f_i')t+\phi_i)}\right\} \\ &= \sum_{i=1}^{70} \mathrm{Re}\left\{s_i(t)\ e^{j(2\pi f_i t+\phi_i)}\right\} \end{aligned} \tag{17}$$

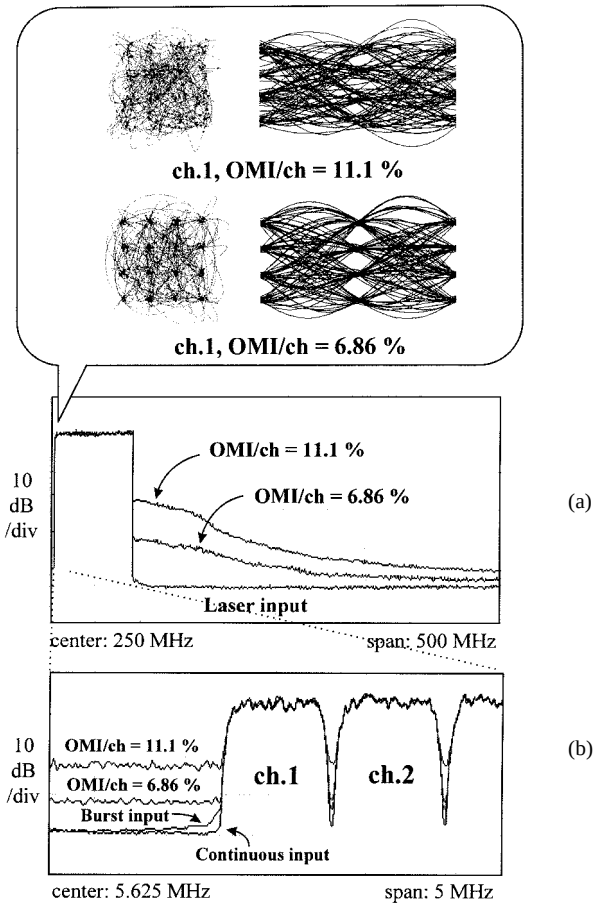

Fig. 11. (a) Spectra of 70 channels of 16-QAM signals before and after modulating a FP laser. Constellation and eye diagrams for OMI/ch = 6.86 and 11.1% are shown for comparison. (b) Spectra of NLD's and transient-induced spectral regrowth right next two channel of channel#1.

which is assumed to be caused by optical reflections in an unisolated laser. All measured results from FP#1, FP#2, and DFB lasers are essentially the same, which indicate that the NLD's induced by strong laser clipping are independent on the type of lasers, and also independent on whether a cooler or an isolator is used (at least at room temperature). It is observed that the analytical and simulation results described in Section II and III match the experimental results very well.

It is interesting to see, from Fig. 12, that a typical FP or DFB laser can transmit more than 1000 QPSK or 170 16-QAM channels even in the presence of strong optical reflections which caused a poor RIN level of -115 dB/Hz. We note that the available data rate per 16-QAM channel is about two times of that for QPSK channel, yet the clipping-limited channel number of 16-QAM modulation is about 0.1 times of that for QPSK modulation, therefore, given sufficient laser bandwidth, QSPK modulation format can transport more information.

V. Discussion

A. Channel Capacity of a Laser Diode Considering Contention-Based MAC Channels

We note that a upstream laser does not have to be operated under a strong-clipping condition, because a reasonable OMI/channel should provide a sufficient optical power budget. However, a upstream laser may have to carry channels using collision-based MAC protocols such as slotted-ALOHA [7], and the original rms OMI/channel may be increased by $\sqrt{k}$ when k users collide in the same contention time slot of a common RF channel. To find out how the channel capacity may be reduced due to the collisions, we assume the worst case that during a short period of time, only one out of a total N channels is operating normally and all the rest $N-1$ channels are suffering collisions (each due to k users). We choose channel#1 with the lowest SNLD as the operating channel. Since k collisions in each channel result in $10\cdot\log(k)$ dB increased power, we let the rms power in channel#1 be $10\cdot\log(k)$ dB less than all the other contention channels. As illustrated in Fig. 13(b), the SNLD requirement of the contention channels should become $16+10\cdot\log(k)$ dB in order for channel#1 to maintain a QPSK SNLD of 16 dB. By using (11) and assuming a RIN level of -115 dB/Hz, we obtain the results shown in Fig. 13(a). We can see that the resultant channel number is dramatically reduced. For example, the maximum number of channels is reduced from 1000 to 125 if $k = 8$, and to 55 if $k = 16$.

Note that the analysis which we have carried out here can also be used to set the dynamic range of multiple input signals (without collisions) under the worst case condition, i.e., $N-1$ equal-power strong channels and a single weak channel. For example, the case of $N = 125$ and $k = 8$ implies that the upstream laser diode can support 124 equal-power strong channels with a single weak channel whose power level is $10 \cdot \log(8)$ or 9 dB lower than all the other channels.

B. Ultimate Channel Capacity in the CATV Downstream Links

The analytical method presented in Section II can also be applied to estimate the ultimate M-QAM channel capacity in a down-stream link. Let us assume $M = 64$ or 256 for each 6 MHz CATV channel, and the first channel starts at 54 MHz. Each QAM signal has a symbol rate of 5 Ms/s and is band-limited by a RRC filter with $\alpha = 0.2$. The results shown in Fig. 14 reveals that even a laser diode with a RIN as high as -135 dB/Hz can transport about 600 channels of 64-QAM and 128 channels of 256-QAM signals, respectively. Note that this channel capacity can be further increased if forward error correction (FEC) codec is used in each channel. If we assume a 30 Mb/s 64-QAM and a 40 Mb/s 256-QAM channel can carry six and nine 4-Mb/s MPEG-II live video channels (with 6 and 4 Mb/s overheads per QAM channel, respectively) [17], the ultimate downstream live-video capacity per clipping-limited laser diode can be 3600 and 1152 channels, respectively. It is interesting to see that 64-QAM modulation can achieve a much higher capacity of video channels, although the required bandwidth on the down-stream laser ($6 \times 600 + 54 = 3654$ MHz) is higher than that for 128 channels of 256-QAM signals ($6 \times 128+54 = 822$ MHz). In estimating this down-stream ultimate capacity with a total signal bandwidth greater than $\sim$1GHz, we are assuming that the dynamic laser nonlinearity is less important when compared to strong-clipping nonlinearity.

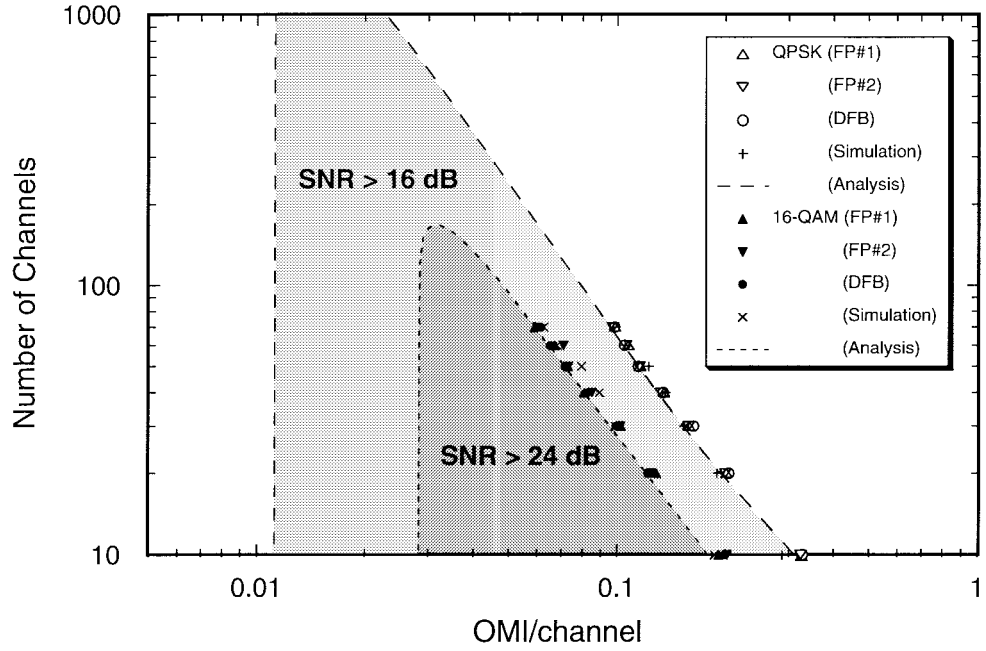

Fig. 12. Number of 1-Ms/s QPSK or 16-QAM channels as a function of OMI/channel. Shaded regions represent where one can find the useful values of OMI/channel and the corresponding transportable number of channels. Left boundaries in both shaded areas are set by RIN $= -115$ dB/Hz.

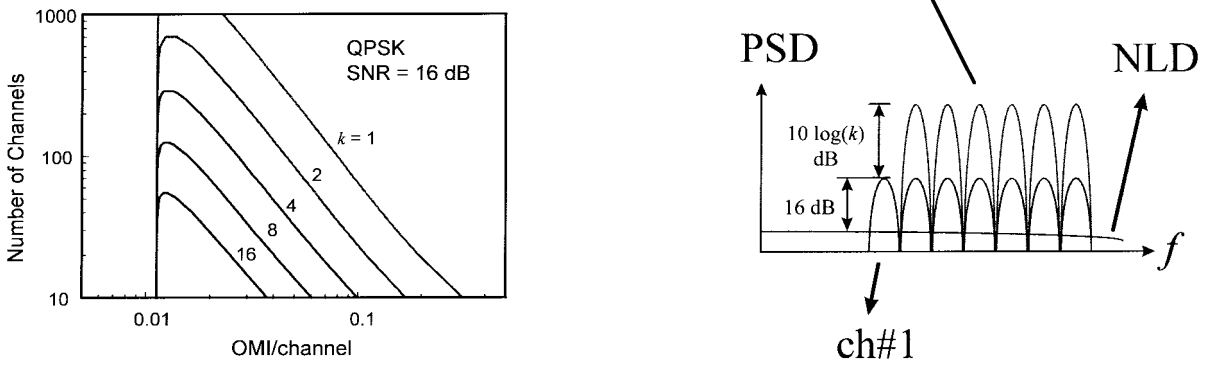

(a) (b)

Fig. 13. (a) Number of 1-Ms/s QPSK channels as a function of OMI/channel for various number of collisions k in all channels but channel#1. (b) Power spectral density (PSD) of the operating channel, channel#1, and the $N-1$ collided channels, and the resultant NLD's.

VI. Conclusion

We have provided a spectral analysis to predict the ultimate M-QAM channel capacity of a laser diode, and have provided verifications for a capacity up to 70 channels of QPSK or 16-QAM signal by building a complete system computer simulation model, and by carrying out experiments using an isolated/cooled DFB laser and two unisolated/uncooled FP lasers. Our analytical results show that for an upstream laser diode, over 1000 1-Ms/s QPSK channels or 170 1-Ms/s 16-QAM channels can be delivered, even in the presence of a high RIN of -115 dB/Hz. However, in investigating the effect of collision-based MAC protocols, we found that, in the worst case condition (collisions occur in all but one channels), the ultimate QPSK channel capacity of an upstream laser diode is dramatically reduced to 125 and 55, for 8 and 16 collisions/channel, respectively. These results have important implications to systems transporting frequency-stacked return-path bands and/or using collision-based MAC channels. As regard to the ultimate capacity of a down-stream laser diode, we found that as high as 600 and 128 channels of 5 Ms/s 64-QAM and 256-QAM signals (equivalent to 3600 and 1152 channels of 4 Mb/s MPEG-II live video signals) can be transported, respectively, assuming a laser RIN level of -135 dB/Hz. These capacities can be further increased to $\sim$24 000 64-QAM and $\sim$4800 256-QAM channels if the downstream laser RIN is -155 dB/Hz.

We have discovered several other important phenomena from our analysis. The first is that when the total modula-

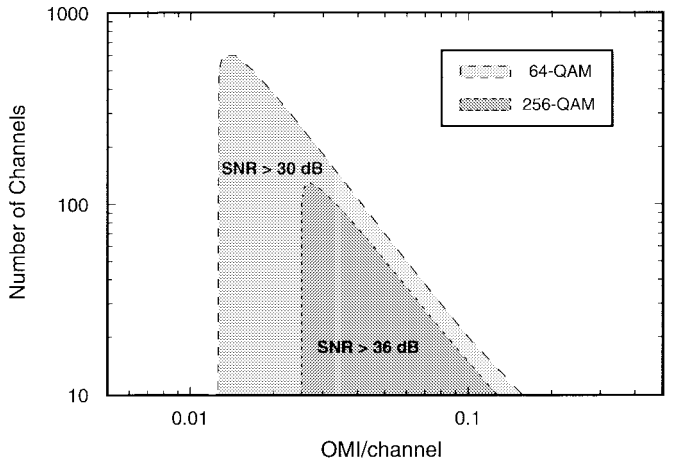

Fig. 14. Number of 5-Ms/s 64/256-QAM channels as a function of OMI/channel (for downstream laser diode). Shaded regions represent where one can find the useful values of OMI/channel and the corresponding transportable number of channels. Left boundaries in both shaded areas are set by RIN $= -135$ dB/Hz.

tion index is greater than 0.45, the dominant NLD under a clipping-limited condition is of the second and third order. However, as the modulation index decreases, the dominant orders increases. These results have important implications to the design of predistortion circuits for the purpose of increasing the channel capacity beyond that of a clipping-limited condition. The second is that we have given an exact estimation of the in-band clipping-induced NLD factor Γ, which can vary significantly with the loading channel number N and the total rms modulation index μ.

In our experiment, we have developed a signal processing technique to generate a maximum number of distinct M-QAM signals by using a computer software and VAWS, for a given speed of DAC's in VAWS. Other interesting phenomena which have been found in our experiments include 1) the fundamental limitation on the digital M-QAM channel capacity of an upstream laser diode is due to strong clipping, and is independent of laser types, i.e., DFB or FP, cooled or uncooled (at least at room temperature), and isolated or unisolated, 2) when the laser is strongly clipped, the spread NLD in multichannel QAM systems can be treated as Gaussian noise instead of impulsive noise (as in weakly clipped downstream laser diode carrying multichannel AM–VSB signals), 3) the transient induced adjacent channel power can be neglected compared to the nonlinear distortion power when the laser diode is strongly clipped.

REFERENCES

[1] A. A. M. Saleh, "Fundamental limit on number of channels in subcarrier-multiplexed lightwave CATV system," *Electron. Lett.*, vol. 25, pp. 776-777, Jun.1989.
[2] K. Alameh and R. A. Minasian, "Ultimate limits of subcarrier multiplexed lightwave transmission," *Electron. Lett.*, vol. 27, pp. 1260-1262, Jul. 1991.
[3] Q. Shi, R. S. Burroughs, and S. Lewis, "An alternative model for laser-clipping induced nonlinear distortion for analog lightwave CATV system," *IEEE Photon. Technol. Lett.*, vol. 4, pp. 784-787, Jul. 1992.
[4] J. E. Mazo, "Asymptotic distortion spectrum of clipped, dc-biased, Gaussian noise," *IEEE Trans. Commun.*, vol. 8, pp. 1339-1344, Aug. 1992.
[5] A. J. Rainal, "Distortion spectrum of laser intensity modulation," *IEEE Trans. Commun.*, vol. 43, pp. 1644-1652, Feb. 1995.
[6] K.-P. Ho and J. M. Kahn, "On models of clipping distortion for lightwave CATV systems," *IEEE Photon. Technol. Lett.*, vol. 8, pp. 125-126, Jan. 1996.
[7] Digital Audio-Visual Council (DAVIC) 1.1 Specifications; IEEE 802.14 Standard Drafts; ITU J.83 Standards.
[8] J. Stroman, "The challenge of return path," *Commun. Eng. Design*, pp. 50-56, Feb. 1995.
[9] S. L. Woodward and G. E. Bodeep, "Uncooled Fabry-Perot lasers for QPSK transmission," *IEEE Photon. Technol. Lett.*, vol. 7, pp. 558-560, May 1995.
[10] P.-Y. Chiang, B. H. Wang, and W. I. Way, "Ultimate capacity of a return-channel laser diode in transporting multi-channel bursty QPSK/16-QAM signals," in *OFC'97 Tech. Dig.*, paper ThP1, Dallas, TX, Feb. 1997.
[11] J. B. Thomas, *An Introduction to Statistical Communication Theory*. New York: Wiley, 1969.
[12] O. Shimbo, *Transmission Analysis in Communication System*, vol. I. Rockville, MD: Computer Science, 1988.
[13] W. I. Way, "Subcarrier multiplexed lightwave system design considerations for subscriber loop applications," *J. Lightwave Technol.*, vol. 7, pp. 1806–1818, Nov. 1989.
[14] N. J. Frigo, M. R. Phillips, and G. E. Bodeep, "Clipping distortion in lightwave CATV systems: models, simulations, and measurements," *J. Lightwave Technol.*, vol. 11, pp. 138–146, Jan. 1993.
[15] P.-Y. Chiang, C. Tai, and W. I. Way, "33-channel 64-QAM signal transmission using a 1.3 μm semiconductor optical amplifier," *IEEE Photon. Technol. Lett.*, vol. 8, pp. 119–121, Jan. 1996.
[16] C. Tai, P.-Y. Chiang, and W. I. Way, "8-way, 70 km transmission of 33-channel 64-QAM signals utilizing 1.3 μm external modulation system and semiconductor optical amplifier," *IEEE Photon. Technol. Lett.*, vol. 8, pp. 1246–1248, Sept. 1996.
[17] A. Murat Tekalp, *Digital Video Processing*. Englewood Cliffs, NJ: Prentice Hall, 1995.

Pi-Yang Chiang (S'95) was born in Taipei, Taiwan, in 1968. He received the B.S. degree in electrical engineering from the National Taiwan University, Tawian, in 1990, and the M.S. degree in communication engineering from the National Cjaio-Tung University, Taiwan, in 1992. He is currently working towards the Ph.D. degree in the National Chiao-Tung University with research interests in hybrid fiber coax networks and subcarrier optical communication systems.

Winston I. Way (S'82–M'83–SM'88) received the B.S. degree from the National Chiao-Tung University, Taiwan, in 1977, and the Ph.D. degree from the University of Pennsylvania, Philadelphia, in 1983.

From 1984 to 1992, he was with Applied Research Division at Bellcore, where he was involved in various lightwave system research projects such as pioneering in distributing satellite, digital radio, and cable television signals by using subcarrier multiplexing techniques; designing hybrid/IC regenerators for direct detection systems; designing lightwave systems that include erbium-doped fiber amplifiers, semiconductor optical amplifiers; studying system issues related to dense wavelength division multiplexing and optical frequency division multiplexing techniques; and studying the feasibility of applying advanced lightwave technologies to SONET/SDH self-healing rings. Since 1992, he has been with the Department of Communications Engineering, the National Chiao-Tung University, Hsinchu, Taiwan, R.O.C., where he is a Professor and has been leading a number of projects on HFC access system technologies and high-speed WDM networking. He has published a book chapter and over 80 refereed technical papers in international journals and conferences and has held three U.S. patents.

Dr. Way has been serving as Chair or Technical Program Committee Member in numerous IEEE/LEOS or IEEE/MTT international conferences and he was an IEEE Journal Guest Editor.